



HAL
open science

Evidence for increased hominid diversity in the Early to Middle Pleistocene of Indonesia

Clément Zanolli, Ottmar Kullmer, Jay Kelley, Anne-Marie Bacon, Fabrice Demeter, Jean Dumoncel, Luca Fiorenza, Frederick Grine, Jean-Jacques Hublin, Nguyen Anh Tuan, et al.

► To cite this version:

Clément Zanolli, Ottmar Kullmer, Jay Kelley, Anne-Marie Bacon, Fabrice Demeter, et al.. Evidence for increased hominid diversity in the Early to Middle Pleistocene of Indonesia. *Nature Ecology & Evolution*, 2019, 3 (5), pp.755-764. 10.1038/s41559-019-0860-z . hal-02296699

HAL Id: hal-02296699

<https://hal.science/hal-02296699>

Submitted on 25 Feb 2021

HAL is a multi-disciplinary open access archive for the deposit and dissemination of scientific research documents, whether they are published or not. The documents may come from teaching and research institutions in France or abroad, or from public or private research centers.

L'archive ouverte pluridisciplinaire **HAL**, est destinée au dépôt et à la diffusion de documents scientifiques de niveau recherche, publiés ou non, émanant des établissements d'enseignement et de recherche français ou étrangers, des laboratoires publics ou privés.

Evidence for increased hominid diversity in the Early-Middle Pleistocene of Indonesia

Clément Zanolli^{1,2*}, Ottmar Kullmer^{3,4}, Jay Kelley^{5,6,7}, Anne-Marie Bacon⁸, Fabrice Demeter^{9,10}, Jean Dumoncel¹, Luca Fiorenza^{11,12}, Frederick E. Grine¹³, Jean-Jacques Hublin¹⁴, Nguyen Anh Tuan¹⁵, Nguyen Thi Mai Huong¹⁵, Lei Pan^{16,17}, Burkhard Schillinger¹⁸, Friedemann Schrenk^{3,4}, Matthew M. Skinner^{14,19}, Xueping Ji^{20,21} & Roberto Macchiarelli^{22,23}

¹Laboratoire AMIS, UMR 5288 CNRS, Université Toulouse III Paul Sabatier, Toulouse, France.

²Laboratoire PACEA, UMR 5199 CNRS, Université de Bordeaux, France. ³Department of Palaeoanthropology, Senckenberg Research Institute and Natural History Museum Frankfurt, Frankfurt a.M., Germany. ⁴Department of Paleobiology and Environment, Institute of Ecology, Evolution, and Diversity, Goethe University Frankfurt, Germany. ⁵Institute of Human Origins and School of Human Evolution and Social Change, Arizona State University, Tempe, USA.

⁶Department of Paleobiology, National Museum of Natural History, Smithsonian Institution, Washington D.C., USA. ⁷Department of Human Evolutionary Biology, Harvard University, Cambridge, USA. ⁸Laboratoire AMIS, UMR 5288 CNRS, Université Paris Descartes, Faculté de chirurgie dentaire, Montrouge, France. ⁹UMR 7206 CNRS, Muséum National d'Histoire Naturelle, Paris, France. ¹⁰Center for GeoGenetics, Copenhagen, Denmark. ¹¹Department of Anatomy and Developmental Biology, Monash University, Melbourne, Australia. ¹²Earth Sciences, University of New England, Armidale, Australia. ¹³Department of Anthropology and Department of Anatomical Sciences, Stony Brook University, Stony Brook, USA. ¹⁴Department of Human Evolution, Max Planck Institute for Evolutionary Anthropology, Leipzig, Germany. ¹⁵Anthropological and Palaeoenvironmental Department, The Institute of Archaeology, Hanoi, Vietnam. ¹⁶Key Laboratory of Vertebrate Evolution and Human Origins, Institute of Vertebrate Paleontology and Paleoanthropology, Chinese Academy of Sciences, Beijing, China. ¹⁷State Key Laboratory of Palaeobiology and Stratigraphy, Nanjing Institute of Geology and Palaeontology, Chinese Academy of Sciences, Nanjing, China. ¹⁸Heinz Maier-Leibnitz Center (FRM-II), Technische Universität München, Garching, Germany. ¹⁹School of Anthropology and Conservation, University of Kent, Canterbury, UK. ²⁰Department of Paleoanthropology, Yunnan Institute of Cultural Relics and Archaeology, Kunming 650118, China. ²¹School of Resource Environment and Earth Science, Yunnan University, Kunming, China. ²²UMR 7194 CNRS, Muséum National d'Histoire Naturelle, Paris, France. ²³Unité de Formation Géosciences, Université de Poitiers, France.

Since the first discovery of *Pithecanthropus (Homo) erectus* by E. Dubois at Trinil in 1891, over 200 hominid dentognathic remains have been collected from the Early-Middle Pleistocene deposits of Java, Indonesia, forming the largest palaeoanthropological collection in Southeast Asia. Most of these fossils are currently attributed to *H. erectus*. However, because of the substantial morphological and metric variation in the Indonesian assemblage, some robust specimens, such as the partial mandibles Sangiran 5 and Sangiran 6a, were formerly variably allocated to other taxa (*Meganthropus palaeojavanicus*, *Pithecanthropus dubius*, *Pongo* sp.). To resolve the taxonomic uncertainty surrounding these and other contentious Indonesian hominid specimens, we used Occlusal Fingerprint Analysis to reconstruct their chewing kinematics, and also used various morphometric approaches based on microtomography to examine internal dental structures. Our results confirm the presence of *Meganthropus* as a Pleistocene Indonesian hominid distinct from *Pongo*, *Gigantopithecus* and *Homo*, and further reveal that

47 **Eugene Dubois' *Homo erectus* paratype molars from 1891 are not hominin (human lineage), but**
48 **instead are more likely to belong to *Meganthropus*.**

49

50 During the Quaternary, episodes of glacial eustasy combined with tectonic uplift and volcanoclastic
51 deposition periodically altered the palaeobiogeography of the Sunda region. These physical and
52 resultant environmental changes facilitated or inhibited intermittent faunal exchanges with the Asian
53 mainland¹ and influenced the evolutionary dynamics of the local faunas, including hominids². The
54 presence of hominids (great apes and humans) in Southeast Asia during the Early and Middle
55 Pleistocene is well documented in the fossil record, with at least three firmly established genera:
56 *Gigantopithecus*, *Pongo* and *Homo*³⁻⁶. The existence of a putative “mystery ape” has also been
57 evoked⁷. Due to the implied vicariance and relict survivorship accompanying these geomorphological
58 events, the appraisal of palaeobiodiversity at a regional scale is difficult. The presence of *Homo* in
59 insular Southeast Asia since the Early Pleistocene has been amply documented by cranial, dental and
60 postcranial remains³. Conversely, apart from four isolated teeth recently discovered in Peninsular
61 Malaysia⁸, only a few dental specimens representing *Pongo* sp. have been reported from the Early
62 and Middle Pleistocene deposits of Indonesia⁹. Because of the convergence in molar crown size and
63 overall morphology between fossil *Homo* and *Pongo*, the taxonomic diagnosis of many Asian Early
64 Pleistocene hominid dentognathic specimens has been debated for over a century, especially
65 concerning isolated teeth and occlusally worn specimens^{10,11} (Supplementary Figure 1 and
66 Supplementary Material). The resulting taxonomic confusion has affected the historical debate on the
67 evolution of the genus *Homo* in Southeast Asia and, more generally, the assessment of Pleistocene
68 hominid palaeobiodiversity⁷.

69 Using three-dimensional virtual imaging, we reassess the taxonomic assignment of two isolated
70 maxillary molars from Trinil (Trinil 11620 and Trinil 11621)^{10,11}, paratypes of *H. erectus*¹², and of the
71 partial mandibles Sangiran 5, the holotype of *Pithecanthropus dubius*¹³, and Sangiran 6a, the holotype
72 of *Meganthropus paleojavanicus*^{14,15}, all currently considered to be *H. erectus*¹⁶⁻¹⁸. We also re-
73 examine the mandibular specimen Arjuna 9, regarded as a robust *H. erectus* similar to Sangiran 6a¹⁹,
74 and seven isolated upper and lower permanent molar crowns from the Early-Middle Pleistocene
75 Sangiran Dome formations (FS-77, SMF-8855, SMF-8864, SMF-8865, SMF-8879, SMF-8898 and
76 SMF-10055), provisionally labelled as *Pongo* sp., but whose taxonomic identity remains problematic
77 (Figure 1, Supplementary Figure 2 and Supplementary Material). The analyses and/or examined
78 features include Occlusal Fingerprint Analysis, enamel distribution and relative enamel thickness,
79 crown-root surface area proportions, enamel-dentine junction topography, and pulp chamber
80 morphology. We compare the results from this Indonesian assemblage with similar data from extant
81 and fossil *Homo* and *Pongo*, as well as the fossil hominids *Sivapithecus* (Late Miocene, South Asia),

82 *Lufengpithecus* (Late Miocene, southern China), and *Gigantopithecus* (Pleistocene, China and
83 Southeast Asia)²⁰ (Supplementary Tables 1-4).

84

85 **Results**

86 One important distinction between humans and non-human apes concerns their dietary ecology and
87 feeding behaviours, reflected in their masticatory apparatus by different morphological adaptations
88 and structural characteristics^{21,22}. Occlusal Fingerprint Analysis²³ of crown wear patterns reveals that
89 all robust Indonesian hominid molars suitable for this investigation (9 of 13) exhibit an ape-like
90 functional macrowear pattern that differs significantly ($p<0.05$) from that of extant and extinct
91 hominin samples, including Javanese *H. erectus* (Figure 2 and Supplementary Table 5). This pattern
92 is characterised by a high dominance of power stroke Phase II over Phase I, evidenced by enlarged
93 Phase II wear facets (Supplementary Table 6). In contrast, humans and extinct hominins, including
94 Chinese and Indonesian *H. erectus*, display proportionately larger buccal Phase I wear facets,
95 indicative of distinct masticatory behaviour (Figure 2).

96 Patterns of enamel distribution are sensitive indicators of dietary adaptations and taxonomic
97 affinities in anthropoids²². Morphometric cartographies distinguish between hominin and ape
98 patterns: in the former, the thickest enamel is deposited on the “functional cusps” rather than on the
99 “guiding” cusps²², while in apes, and notably in *Pongo*, it lies at the periphery of the occlusal basin²⁴⁻
100 ²⁶. Our analyses reveal that all but one of the modestly worn hominid molars from Java (n=8) show
101 an ape pattern. The maxillary molar Trinil 11620 displays even relatively thicker enamel at the
102 periphery of the occlusal basin than is typically found in *Pongo*, more closely approximating the
103 Miocene apes *Sivapithecus* and *Lufengpithecus* (Figure 3). Conversely, the lower molar specimen
104 SMF-8865 closely resembles the condition characterising African and Indonesian *H. erectus*, showing
105 the thickest enamel localized on the buccal cusps, while Arjuna 9, FS-77, SMF8855, SMF-8864 and
106 SMF-8879 have the thickest enamel distributed along the marginal ridges around the occlusal basin.
107 Crown tissue proportions, including the commonly used Relative Enamel Thickness index^{24,26,27},
108 overlap across all extinct and extant samples and do not discriminate the Javanese robust specimens
109 (Supplementary Figure 3 and Supplementary Tables 7-8).

110 Crown-root surface area proportions have also been demonstrated to show a strong phylogenetic
111 signal, independent of feeding adaptations in tooth morphology²⁸. Both upper molars from Trinil and
112 the lower post-canine teeth of Sangiran 6a and Arjuna 9 exhibit proportionally large root surfaces
113 compared to the lateral (non-occlusal) crown area, resembling pongines and *Lufengpithecus* and
114 differing substantially from *Homo* (Figure 4, Supplementary Figure 4 and Supplementary Table 9).

115 The topography of the enamel-dentine junction (EDJ), which reliably distinguishes fossil and
116 extant hominid taxa^{24,26,29}, approximates the inner enamel epithelium of the developing tooth and

117 provides useful information about taxon-specific processes underlying crown growth²⁹. Six of the
118 Javanese lower molars show a cingulum-like, mesiodistally extended buccal protostylid at the EDJ,
119 which is distinct from the morphology commonly found in *Homo* and *Pongo* but similar to the
120 condition expressed by the Miocene Chinese ape *Lufengpithecus* (Supplementary Figure 5; see also
121 Supplementary Figure 6 for the lower P4 EDJ morphology). The specimen SMF-8865 does not show
122 the same coarse wrinkling pattern at the EDJ as the other robust Indonesian hominids, or the dense
123 crenulation pattern typical of *Pongo*, but rather resembles the *H. erectus* condition (Supplementary
124 Figure 5).

125 We also performed geometric morphometric (GM) analyses of the molar EDJ to compare the
126 Indonesian fossil specimens to an assemblage of fossil and extant hominids (Figure 5). The results
127 show statistical discrimination between *Pongo* and *Homo* and unambiguously classify the robust
128 Javanese specimens as non-human apes, again with the exception of SMF-8865 (Supplementary
129 Table 10). Indeed, except for the latter specimen, the EDJ shape of this Javanese sample of robust
130 teeth is distinguished from *Homo* and overlaps those of *Pongo* and *Lufengpithecus*, even if some
131 specimens like the holotype of *Meganthropus*^{14,15}, Sangiran 6a, are outside the variation of *Pongo*
132 (Figure 5, Supplementary Figure 7). As in fossil *Pongo*²⁴, *Gigantopithecus*²⁴, *Sivapithecus* and
133 *Lufengpithecus*, the EDJ of these teeth consistently exhibits a low topography with higher mesial than
134 distal dentine horns. Interestingly, comparable results are obtained when the same analysis is
135 performed on the lower P4 of Sangiran 6a (Supplementary Figures 8-9 and Supplementary Table 11).
136 Conversely, in *Homo*^{26,29} and in SMF-8865 as well, the EDJ typically shows higher relief, with
137 dentine horns of sub-equal height and more distally-set buccal cusps (Figure 5). In light of this, it is
138 noteworthy that a pongine-like endostructural signature (but different from that typical of *Pongo*) was
139 recently identified in an isolated deciduous mandibular molar from the Early Pleistocene of Sangiran
140 that was originally labelled as *Meganthropus*¹⁴, but later allocated to early *Homo* (rev. in ref. 26).

141 While the taxonomic significance of the EDJ is supported by previous studies²⁹, that of pulp
142 chamber shape has not been systematically evaluated. However, marked morphological differences
143 are notable in the height, thickness and shape of the pulp chamber between fossil and extant hominid
144 taxa (Supplementary Figures 10-11). Accordingly, we performed a preliminarily GM analysis limited
145 to the four extant hominid genera. Our results demonstrate that *Homo* and *Pongo* are statistically
146 distinguished by pulp chamber morphology (Supplementary Material and Supplementary Figure 12).
147 Based on these results, three-dimensional landmark-based analyses of the shape of the pulp chamber
148 (not possible for SMF-8865) were thus extended to the fossil specimens. Similar to the analyses of
149 the EDJ, they clearly discriminate the robust Javanese specimens from *Homo* (Supplementary Table
150 10). However, in contrast to the results of EDJ shape, the shape of the pulp chamber also distinguishes
151 most of the fossil specimens forming the Javanese assemblage from *Pongo* (except for SMF-8879)

152 and approximates *Lufengpithecus* (Figure 5 and Supplementary Figure 13).

153 When only non-hominin taxa are considered in the GM analyses of the EDJ and pulp chamber, the
154 robust Indonesian molars are generally distinguished from *Pongo* (except for SMF-8879, which falls
155 close to or within the *Pongo* range of variation) and approximate the Miocene representatives,
156 especially *Lufengpithecus* (Figure 6 and Supplementary Figures 14-15).

157

158 **Discussion**

159 Previous attempts to sort the Indonesian hominid dentognathic remains into morphs primarily based
160 on their external morphology provided different, sometimes contradictory, results^{7,18,19,30}. This is
161 because the fossil assemblage shows variable preservation conditions and most dental remains are
162 affected by extensive occlusal wear (Supplementary Figure 1). Based on multiple aspects of dental
163 morphology, our re-analysis of this long-controversial sample of robust Pleistocene dentognathic
164 specimens from Java demonstrates that, with the exception of the isolated crown SMF-8865, which
165 we attribute to *H. erectus*, all the specimens investigated here most likely represent non-hominin
166 species. Moreover, Trinil 11620, Trinil 11621, Sangiran 5, Sangiran 6a, Arjuna 9, FS-77 and SMF-
167 8864 are dentally distinct from *Pongo* and represent a third ape lineage in addition to *Pongo* and
168 *Gigantopithecus* that survived beyond the Miocene in South-eastern Asia. We propose to allocate this
169 material to the resurrected species *Meganthropus palaeojavanicus* von Koenigswald, 1950^{14,15}, but
170 as a non-hominin. The holotype is Sangiran 6a and the other specimens are paratypes. Consequently,
171 *Pithecanthropus dubius*¹⁵ becomes a junior synonym of *Meganthropus palaeojavanicus*.

172 Unlike most apes, Sangiran 6a and Sangiran 9¹⁴⁻¹⁷ lack the canine/P3 honing complex and the P3
173 is non-sectorial, being more similar to the P4 with reduced crown height, a relatively prominent
174 metaconid (thus being clearly bicuspid) and a more buccolingually oriented crown major axis. In all
175 these features, *Meganthropus* is similar to Plio-Pleistocene hominins, which might argue for
176 *Meganthropus* being a hominin rather than a non-hominin hominid as we conclude from our analysis
177 of internal dental structure. However, there are other fossil apes in which the P3 is non-sectorial and
178 converges on a hominin-like morphology, most strikingly among megadont species that have
179 undergone marked canine reduction, such as the Late Miocene *Indopithecus*³¹, and especially the
180 Pleistocene *Gigantopithecus*^{6,32}, in which the P3 is typically bicuspid. A relatively low-crowned and
181 more transversely oriented P3 associated with some degree of canine reduction (at least with respect
182 to its cervical dimensions) also characterises the Late Miocene megadont *Ouranopithecus*³³. While
183 having a sectorial P3, *Lufengpithecus* also shows strong expression of the metaconid, in some cases
184 bordering on a bicuspid morphology³⁴.

185 Concerning Trinil 11620, this tooth was among those in another recent attempt to sort out the
186 identities of Pleistocene dental remains, mostly from China but including several teeth from Southeast

187 Asia as well¹¹. Other than 2D enamel thickness and EDJ topography, that study examined different
188 aspects of dental morphology than those examined here, and, with the exception of Trinil 11620, on
189 an entirely different sample. While Trinil 11620 is identified *a priori* as a hominin in that study and
190 another previous study^{11,35}, this is based on a prior analysis¹⁰ to decide only whether it should be
191 assigned to *Homo* or *Pongo*, without considering the possible presence of an additional Pleistocene
192 ape lineage in Southeast Asia in addition to *Pongo* and *Gigantopithecus*. Also, no results or
193 conclusions are reported for it other than a long-period (Retzius) developmental line periodicity of
194 either 6 or 7¹⁰. These values are well below the reported range of periodicities for fossil or extant
195 *Pongo* and a value of 6 would be an unusually low value for fossil or extant *Homo*^{11,35,36}. While
196 *Gigantopithecus* and *Sivapithecus* typically show values of 8-11 days^{11,37}, we note that in a small
197 sample of *Lufengpithecus*, the Retzius line periodicity is 7-9 days³⁸. Although we did not examine
198 long-period line periodicity, and there is substantial variation in long-period line periodicities in
199 hominid taxa^{35,36}, the low value for Trinil 11620 could perhaps be considered as additional support
200 for the assignment of this tooth to *Meganthropus*.

201 In keeping with its prior definition, *Meganthropus* is distinguished from *Homo* by having
202 absolutely large teeth^{14,15}, a mandibular corpus with a thick and rounded inferior border, a large
203 extramolar sulcus and strong lateral prominence¹⁵⁻¹⁷, molarised premolars, and low molar crowns
204 with coarse wrinkling converging toward the centre of the occlusal surface^{14,15}. Our results
205 demonstrate that *Meganthropus* is further distinguished from *Homo* by an ape-like molar occlusal
206 macrowear pattern, peripherally-distributed thicker molar enamel, a low crowned EDJ with relatively
207 short dentine horns, a particularly slender pulp shape with high horns, and lower crown/root surface
208 area proportions. It further differs from penecontemporaneous *H. erectus* by the presence of a
209 cingulum-like protostylid in both the enamel and the underlying EDJ. This feature is commonly found
210 in *Australopithecus* and *Paranthropus*, but *Meganthropus* differs from these two hominins by its ape-
211 like occlusal wear pattern (Supplementary Figure 16), thicker peripheral enamel (whereas thicker
212 enamel is found at the cusp tip in australopiths³⁹), the lower EDJ topography, and more slender pulp
213 chamber with vertically elongated pulp horns (Supplementary Figure 17). As a further consequence
214 of recognising *Meganthropus* as non-hominin, certain features commonly regarded as characteristic
215 of hominins, such as the loss of the canine/P3 honing complex, lack of a marked mandibular simian
216 shelf, moderately mesiodistally elongated premolars with a double root and premolar/molar size
217 proportions^{12,14-17}, more likely represent homoplastic traits in *Meganthropus*. From our results, it is
218 also evident that, aside from marked differences in mandibular morphology and proportions,
219 *Meganthropus* differs from *Pongo* by having laterally-positioned molar dentine horns, a slender pulp
220 chamber, and a cingulum-like expression of the protostylid (Figure 6 and Supplementary Figures 5
221 and 10). *Meganthropus* is also clearly distinct from *Gigantopithecus*, the latter displaying higher-

222 crowned and narrower molars with low bulbous cusps and rounded crests, a large cuspule formed by
223 a lobe between the protoconid and metaconid giving the lower molars a distinctive cusp pattern
224 comprised of two pairs of main cusps arranged peripherally, a line of smaller midline cusps that
225 includes the talonid cuspule and the hypoconulid, the lack or faint expression of the protostylid, strong
226 buccolingual mid-crown waisting⁶, thicker occlusal enamel, and higher EDJ topography²⁴ (for a
227 detailed differential diagnosis of *Meganthropus*, see Supplementary Material section 3,
228 Supplementary Figure 18 and Supplementary Table 12).

229 We provisionally assign SMF-8879 to *Pongo* sp. Future analyses should clarify the taxonomic
230 status of the specimens SMF-8855, SMF-8898 and SMF-10055, currently regarded as pongines, but
231 which also share some features with the Asian Miocene apes, as well as other specimens from Early
232 Pleistocene Java whose status continues to be debated (e.g., Sangiran 8, Sangiran 9, Sangiran 27)^{16,17}.

233 Across most of Eurasia, apes became extinct prior to the end of the Miocene. They survived into
234 the Pleistocene only in South-eastern Asia, represented by *Gigantopithecus* and *Pongo*, both known
235 from southern-most China into Southeast Asia^{5,40}. To these can be added *Meganthropus* from Java,
236 formerly suggested to be an ape by some^{12,14,15} but only confidently demonstrated to be so by the
237 comparative analyses presented here. As demonstrated by paleobotanical, paleontological and
238 geochemical proxies^{2,41-43}, the Early to Middle Pleistocene palaeoenvironments of Sangiran and Trinil
239 included a variety of mixed and temporally shifting habitats, ranging from open woodland areas to
240 dense forests capable of supporting the presence of multiple large-bodied hominid species in addition
241 to at least two arboreal monkeys, *Macaca fascicularis* and *Trachypithecus cristatus*². Of the other
242 apes present during the late Miocene in South and Southeast Asia - *Sivapithecus*, *Khoratpithecus*, and
243 *Lufengpithecus* - *Meganthropus* appears to be dentally most similar to the last, evidenced by the
244 presence in both of low-cusped and wrinkled molar crowns^{21,44,45} with a squat EDJ, an extended
245 protostylid and a slender pulp chamber (Figure 5, Supplementary Figures 5 and 10). In contrast,
246 *Sivapithecus* and *Khoratpithecus* have higher, more bunodont molars with marked mid-crown
247 buccolingual constriction^{21,22} and *Sivapithecus* has proportionally higher dentine horns (Figure 5). In
248 sum, when combining evidence from the occlusal wear pattern, internal tooth structure, and aspects
249 related to dental development¹⁰, *Meganthropus* shows greatest affinity to *Lufengpithecus*, and we
250 hypothesize that these taxa are phylogenetically closely related. Substantiating this will require fuller
251 knowledge than currently available of character polarity and homology versus homoplasy in features
252 of tooth internal structure and dental development as a whole.

253

254 **Conclusion**

255 During the Early-Middle Pleistocene, at least three and perhaps four hominid genera inhabited what
256 is now Indonesia: *Homo*, *Pongo* and *Meganthropus*, with the possible presence of *Gigantopithecus*⁴⁰.

257 This is a higher level of diversity than previously recognised and, with the newly resurrected genus
258 *Meganthropus* now recognized as an ape, is particularly noteworthy for the late survival of two to
259 three large ape lineages. Whether related to the expansion of *H. erectus*, palaeoenvironmental
260 changes, competition with *Pongo* or *Gigantopithecus*, or some combination of these factors,
261 *Meganthropus* did not persist beyond the Middle Pleistocene, leaving only three species of the genus
262 *Pongo* (*P. pygmaeus*, *P. abelii* and *P. tapanuliensis*) subsisting today in remote and protected
263 Indonesian localities⁴⁶.

264

265 **Methods**

266 **X-ray and neutron microtomography.** Except for the Trinil molars and Sangiran 5 (see below), all
267 Javanese hominid specimens studied here (Sangiran 6a, Arjuna 9, FS-77, SMF-8855, SMF-8864,
268 SMF-8865, SMF-8879, SMF-8898 and SMF-10055) were scanned using the X-ray microfocus
269 sources (X- μ CT) at: the Helmholtz-Zentrum Berlin (equipment CONRAD II instrument), the
270 Department of Human Evolution of the Max Plank Institute of Leipzig (equipment BIR ACTIS
271 225/300), the University of Poitiers (equipment X8050-16 Viscom AG), and the Seckenberg
272 Research Institute (Phoenix Nanotom s 180). Acquisitions were performed according to the
273 following parameters: 100-160 kV, 0.11-90 μ A, 0.14-0.36° of angular step. The final volumes were
274 reconstructed with voxel sizes ranging from 20.8 to 40.7 μ m. The two Trinil molars (11620 and
275 11621) were scanned by SR- μ CT on beamline ID 19 of the European Synchrotron Radiation
276 Facility at Grenoble using absorption mode with an isotropic voxel size of 31.12 μ m³ at an energy
277 of 60 keV¹⁰. The dataset of 632 images is available in 8 bits .tif format at the ESRF Paleontological
278 Database (<http://paleo.esrf.eu>). The X- μ CT acquisitions of the comparative fossil and extant
279 hominid specimens were performed using various equipment with the following parameters: 95-145
280 kV, 0.04-0.40 μ A, 0.17-0.36° of angular step. The final volumes were reconstructed with voxel
281 sizes ranging from 8.3 to 60.0 μ m.

282 The specimens Sangiran 5 and Sangiran 6a were scanned by neutron microtomography (n-
283 μ CT)⁴⁷⁻⁵¹ at the ANTARES Imaging facility (SR4a beamline) of the Heinz Maier-Leibnitz Center
284 (FRM II) of Technische Universität München. The neutron beam originated from the cold source of
285 the FRM II reactor, with an energy range mostly from 3 to 20 meV, a collimation ratio of L/D=500
286 (ratio between sample-detector distance and collimator aperture) and an intensity of 6.4 x 10⁷
287 n/cm²s. A 20 μ m Gadox screen was used to detect neutrons. Both a cooled scientific CCD camera
288 (Andor ikon-L) and cooled scientific CMOS camera (Andor NEO) were used as detectors. The final
289 virtual volume of these specimens was reconstructed with an isotropic voxel size of 20.45 μ m.

290

291 **Data processing.** Some specimens showed low contrast between the enamel and dentine in some

292 parts of the dataset, precluding automatic segmentation. In such cases, enamel and dentine were
293 segmented using the magic wand tool in Avizo 8.0 (FEI Visualization Sciences Group) and manual
294 corrections were locally applied. Use of the interpolation tool was limited to areas where the
295 distinction between enamel and dentine could not be precisely demarcated. A volumetric
296 reconstruction was then generated for each specimen. In most cases, the contrast resolution enabled
297 carrying out a semi-automatic threshold-based segmentation following the half-maximum height
298 method (HMH⁵²) and the region of interest thresholding protocol (ROI-Tb⁵³) taking repeated
299 measurements on different slices of the virtual stack⁵⁴. Because the detection of the tissue interfaces
300 is based on attenuation at the boundary of a structure in both X-ray and neutron-based
301 microtomography, we performed a threshold-based segmentation with manual corrections, as
302 usually applied for X-ray acquisitions^{55,56}. We quantified the degree of morphological and
303 dimensional coherence between the X-ray microtomography (X- μ CT) and n- μ CT datasets of
304 Sangiran 6a. The superimposed EDJ based on the X- μ CT and n- μ CT records show maximum 240
305 μ m differences and an average of 65.7 μ m variation (Supplementary Figure 19). Considering the
306 difference in voxel size of the two original datasets (39.33 μ m and 20.45 μ m for the X-ray and
307 neutron data, respectively), the differences in LM1 enamel volume (349.26 μ m³ and 346.61 μ m³),
308 dentine-pulp volume (529.1 μ m³ and 526.7 μ m³) and crown volume (878.4 μ m³ and 873.3 μ m³) are
309 less than 1% and can be regarded as negligible.

310

311 **Occlusal Fingerprint Analyses.** The analysis of dental wear facets enables the reconstruction of
312 occlusal behaviour²³. Qualitative wear facet analysis performed by Mills⁵⁷ already led to the
313 conclusion that in primates and insectivores the occlusal power stroke of the chewing cycle consists
314 of two phases (buccal Phase and lingual Phase), which were later determined as Phase I and Phase
315 II^{58,59}. The chewing cycle starts with the preparatory (closing) stroke where three-body contact
316 (tooth-food-tooth) leads to puncture-crushing activity with rare contacts of antagonistic crowns.
317 Real chewing starts with Phase I⁵⁹, in which during stereotypic cycles tooth-tooth contacts may
318 occur more commonly, producing guiding buccal and lingual Phase I facets through shearing
319 activity along the buccal slopes of the buccal and lingual cusps of the lowers and complementary
320 facets on the lingual cusp slopes of the upper molars. Phase I ends in maximum intercuspation
321 (centric occlusion) leading into Phase II with a more or less lateral shift of the lower jaw leading to
322 grinding activity until the last antagonistic contacts. During the recovery stroke the jaws open with
323 no dental contacts^{23,25,59}. The Phase I and Phase II pathway of the power stroke is recorded in the
324 wear facet pattern on the occluding molars^{23,60-63}. To assess the occlusal motion pattern(s)
325 characteristic of the Early Pleistocene robust Javanese hominid teeth considered here, we applied
326 Occlusal Fingerprint Analysis (OFA) to attribute proportions of wear facet areas to power stroke

327 phases in order to compare occlusal motion patterns in a sample of extant and fossil Asian great
328 apes and *Homo*. Occlusal macrowear areas, including wear facets following Maier and Schneck⁶⁰,
329 were identified on virtual surface models of upper and lower molar crowns following the OFA
330 method described in Kullmer et al.²³ and Fiorenza et al.⁶⁴. The 3D surface data acquisition derived
331 either from μ CT datasets or from 3D surface scanning with a smartSCAN-HE (Breuckmann
332 GmbH). Scans were taken either from originals or from high resolution casts that provide
333 reasonable resolution of macrowear for mapping wear facet areas⁶¹. We used the modular software
334 package PolyWorks® 2016 (InnovMetric Inc.) to edit the surface models. The polyline tool in the
335 software module IMEdit was applied to interactively mark and fit closed polylines onto the model
336 surfaces along the perimeter of wear facets in each tooth crown. By re-triangulation of the crown
337 surfaces, the polylines became integrated into the surface models. To measure each wear facet area,
338 triangles were selected up to each polyline curve, grouped and color-coded following the occlusal
339 compass^{23,62}. The area measurement tool in IMEdit was used to compute area in mm² for each wear
340 facet. Wear facet areas were summed for chewing cycle power stroke phases^{59,65}. Buccal Phase 1
341 (BPh I), lingual Phase 1 (LPh I) and Phase 2 (Ph II) facet area data were grouped for comparing
342 percentage distribution of wear. To compare power stroke movements only, flat worn areas on cusp
343 tips, identified as tip crushing areas⁶⁴, were excluded because this type of tissue loss usually results
344 from puncture-crushing activity^{59,65} and is not attributable with certainty to one of the two power
345 stroke phases. Percentage results are illustrated in ternary plots. Each corner of the triangle
346 represents 100% of one variable. Accordingly, a sample with an equal distribution of wear facet
347 areas will be placed in the centre of the triangle. The plots were generated using the ggtern package
348 v.2.2.2⁶⁶ in R v.3.4⁶⁷. The R package RVAideMemoire 0.9-66⁶⁸ was used to perform one-way
349 permutational multivariate analysis of variance (PERMANOVA) on the three variables (BPh I, LPh
350 I and Ph II) separately for the maxillary and mandibular molar samples. A Bray-Curtis similarity
351 matrix was calculated based on a 9999 permutations parameter. For both upper and lower molars
352 the test was significant ($p < 0.05$), with values for the pseudo-F model of 18.78 and 13.98 and R²
353 coefficients of 0.53 and 0.57, respectively. Post-hoc PERMANOVA pairwise comparisons were run
354 with a false discovery rate (FDR) correction (Supplementary Table 5).

355

356 **3D tooth tissue proportions.** Premolar and molar crowns and roots were digitally isolated at the
357 cervix along the best-fit plane and surface rendering was performed using unconstrained smoothing
358 for visualization, while constrained smoothing was applied for the quantitative analyses. For the
359 molar teeth, seven linear, surface, and volumetric variables describing tooth tissue proportions were
360 digitally measured or calculated on the molars: Ve, the volume of the enamel cap (mm³); Vcdp; the
361 volume of the crown dentine+pulp (mm³); Vc, the total crown volume; SEDJ, the surface area of

362 the enamel-dentine junction (mm^2); $V_{\text{cdp}}/V_{\text{c}}$, the percent of the crown volume that is dentine and
363 pulp (%); 3D AET ($=V_{\text{e}}/\text{SEDJ}$), the three-dimensional average enamel thickness (mm); 3D RET
364 ($=3\text{D AET}/V_{\text{cdp}}^{1/3} \times 100$), the scale-free three-dimensional relative enamel thickness (see
365 methodological details in refs. 24,36,69). For both premolars and molars, the following parameters
366 were also calculated: LEA, the lateral enamel surface area (mm^2)⁷⁰; RA, the total root surface area
367 (mm^2)⁷⁰; CRR ($=\text{LEA}/\text{RA} \times 100$), the crown-root ratio (%) (see Figure 4, Supplementary Figures 3-4
368 and Supplementary Tables 3,4,7,8). Because of the advanced degree of occlusal wear in Sangiran
369 6a, only crown-root proportions were assessed for the mandibular fourth premolar.

370 Intra- and interobserver accuracy tests of the measures run by two observers provided differences
371 $<5\%$. Adjusted Z-score analyses^{71,72} were performed on three tooth crown tissue proportions
372 parameters ($V_{\text{cdp}}/V_{\text{c}}$, 3D AET and 3D RET) for the robust Indonesian hominid maxillary (Trinil
373 11620, Trinil 11621 and SMF-8898) and mandibular molars (Arjuna 9, FS-77, SMF-8855, SMF-
374 8864, SMF-8865, SMF-8879 and SMF-10055) and were compared with extant and fossil hominid
375 samples (Supplementary Figure 20 and Supplementary Table 8). This statistical test was also
376 applied for the CRR parameter on the maxillary molars Trinil 11620 and Trinil 11621, on the
377 mandibular fourth premolar of Sangiran 6a and on the molars of Sangiran 6a and Arjuna 9
378 preserving complete roots (Figure 4, Supplementary Figure 4 and Supplementary Table 9). This
379 statistical method allows the comparison of unbalanced samples, which is often the case when
380 dealing with the fossil record, using the Student's t inverse distribution following the formula: $[(x-$
381 $m)/(s \times \sqrt{1+1/n})]/(\text{Student.t.inverse}(0.05;n-1))$, where x is the value of the variable; m is the mean
382 of the same variable for a comparative sample; n is the size of the comparative sample; and s is the
383 standard deviation of the comparative sample.

384

385 **Enamel thickness distribution cartographies.** The 3D topographic mapping of site-specific
386 enamel thickness variation was generated from the segmented enamel and crown dentine
387 components of unworn to only slightly worn teeth and rendered using chromatic scales⁷³⁻⁷⁷. A
388 rainbow chromatic scale was also used to illustrate gradual variation of enamel thickness, ranging
389 from the thickest (in red) to the thinnest (in blue) (Figure 3).

390

391 **Geometric morphometric analyses.** 3D geometric morphometric (GM) analyses were conducted
392 on the virtual surfaces of the EDJ of the maxillary molars and mandibular fourth premolar and
393 molars. The landmarks were set along the marginal outline of the EDJ occlusal basin⁷⁷. For the
394 maxillary molars, six landmarks were set: three at the apex of the paracone, protocone and
395 metacone dentine horns, and three at each intermediate lowest point between two horns along the
396 dentine marginal ridges and oblique crest. For the lower fourth premolar, eight landmarks were

397 placed on the EDJ surface: four at the apex of the protoconid, metaconid, entoconid and hypoconid
398 dentine horns and four at each intermediate lowest point between two horns along the dentine
399 marginal ridge. For the mandibular molars, seven landmarks were placed: four at the apex of the
400 protoconid, metaconid, entoconid and hypoconid dentine horns and three at each intermediate
401 lowest point between two horns along the dentine marginal ridge (located by translating the cervical
402 plane occlusally), except between the two distal horns (because of the variable presence of the
403 hypoconulid, notably in modern humans, this cusp and the distal marginal ridge were not
404 considered). While the specimen Trinil 11620 is virtually unworn, the protocone dentine horn apex
405 of Trinil 11621 is affected by wear. It was thus reconstructed based on the intact height and
406 morphology of the paracone, as well as on those of the mesial dentine horns of Trinil 11620. A
407 similar procedure was applied to reconstruct the buccal dentine horns of Sangiran 5 and Sangiran 6a
408 (Figure 1). We also conducted GM analyses on pulp chamber shape, setting similarly located
409 landmarks on the cavity roof of the maxillary and mandibular molars, but not on that of the lower
410 premolar because of a lack of expression of the distal cusps on its pulp chamber. We performed
411 generalized Procrustes analyses, principal component analyses (PCA) and between-group principal
412 component analyses (bgPCA) based on the Procrustes shape coordinates⁷⁸ and using genera as
413 groups (Figures 5-6 and Supplementary Figures 9-11 and 13-15). The robust Indonesian hominid
414 specimens were included a posteriori in the bgPCA. The analyses were performed using the
415 package *ade4* v.1.7-6⁷⁹ for R v.3.4⁶⁷. Allometry was tested using multiple regressions⁸⁰ in which the
416 explanatory variable is the centroid size and the dependent variables are the PC and bgPC scores. In
417 all PCA and bgPCA, the first components only show a weak allometric signal ($0.00 < R^2 < 0.30$), the
418 differences between specimens thus mostly representing shape-variation. In order to statistically
419 assess the taxonomic affinities of the robust Indonesian hominid molars, we used a supervised
420 classification method by Support Vector Machine (SVM). Compared with linear discriminant
421 analyses (LDA) and quadratic discriminant analyses (QDA), SVM makes no assumptions about the
422 data, meaning it is a very flexible and powerful method⁸¹. SVM tests were performed on the PC
423 scores from each GM analysis on the number of PCs needed to achieve more than 95% of the total
424 variability (i.e., 6 to 11 PCs) (Supplementary Tables 5 and 11). Leave-2-out cross-validations were
425 run in order to validate the model (predictive accuracy) of classification for the groups including
426 hominins (*Homo*) on the one hand and apes (*Ponginae-Lufengpithecus*) on the other. We then tested
427 the attribution of the Indonesian fossil hominid specimens included in the GM analyses (Arjuna 9,
428 Sangiran 5, Sangiran 6a, FS-77, SMF-8855, SMF-8864, SMF-8865, SMF-8879, SMF-8898, SMF-
429 10055, Trinil 11620, Trinil 11621) with respect to the model.

430

431 **Data availability.** The authors declare that all data supporting the findings of this study are

432 available within the paper [and its Supplementary information files].

433

434 **References**

- 435 1. Voris, H.K. Maps of Pleistocene sea levels in Southeast Asia: shorelines, river systems and time
436 durations. *J. Biogeogr.* **27**, 1153-1167 (2000).
- 437 2. Larick, R. & Ciochon, R.L. Early hominin biogeography in island Southeast Asia. *Evol.*
438 *Anthropol.* **24**, 185-213 (2015).
- 439 3. Antón, S.C., Spoor, F., Fellmann, C.D. & Swisher III, C.C. in *Handbook of Paleoanthropology*
440 (eds Henke, W. & Tattersall, I.) 1655-1695 (Springer, New York, 2007).
- 441 4. Ciochon, R.L. in *Out of Africa I: The first hominin colonization of Eurasia* (eds Fleagle, J.G.,
442 Shea, J.J., Grine, F.E., Baden, A.L. & Leakey, R.E.) 111-126 (Springer, Dordrecht, 2010).
- 443 5. Harrison, T., Jin, C., Zhang, Y., Wang, Y. & Zhu, M. Fossil *Pongo* from the Early Pleistocene
444 *Gigantopithecus* fauna of Chongzuo, Guangxi, southern China. *Quat. Intl.* **354**, 59-67 (2014).
- 445 6. Zhang, Y. & Harrison, T. *Gigantopithecus blacki*: a giant ape from the Pleistocene of Asia
446 revisited. *Am. J. Phys. Anthropol.* **162**, 153-177 (2017).
- 447 7. Ciochon, R.L. The mystery ape of Pleistocene Asia. *Nature* **459**, 910-911 (2009).
- 448 8. Ibrahim, Y.K. *et al.* First discovery of Pleistocene orangutan (*Pongo* sp.) fossils in Peninsular
449 Malaysia: Biogeographic and paleoenvironmental implications. *J. Hum. Evol.* **65**, 770-797
450 (2013).
- 451 9. Kaifu, Y., Aziz, F. & Baba, H. New evidence of the existence of *Pongo* in the Early/Middle
452 Pleistocene of Java. *Geol. Res. Dev. Centre Bandung* **27**, 55-60 (2001).
- 453 10. Smith, T.M. *et al.* Taxonomic assessment of the Trinil molars using non-destructive 3D
454 structural and development analysis. *PaleoAnthropol.* **2009**, 117-129 (2009).
- 455 11. Smith, T.M. *et al.* Disentangling isolated dental remains of Asian Pleistocene hominins and
456 pongines. *PLoS One* **13**, e0204737 <https://doi.org/10.1371/journal.pone.0204737> (2018).
- 457 12. Dubois, E. *Pithecanthropus erectus, eine menschenaehnliche Uebergangsform aus Java.*
458 Landesdruckerei, Batavia (1894).
- 459 13. Tyler, D.E. Sangiran 5, ("*Pithecanthropus dubius*"), *Homo erectus*, "*Meganthropus*", or *Pongo*?
460 *Hum. Evol.* **18**, 229-242 (2003).
- 461 14. von Koenigswald, G.H.R. Fossil hominids of the Lower Pleistocene of Java: Trinil. *18th Intl.*
462 *Geol. Congr.* **9**, 59-61 (1950).
- 463 15. Weidenreich, F. Giant early man from Java and South China. *Anthropol. Pap. Am. Mus. Nat.*
464 *Hist.* **40**, 1-134 (1945).
- 465 16. Kaifu, Y. *et al.* Taxonomic affinities and evolutionary history of the Early Pleistocene Hominids
466 of Java: Dentognathic evidence. *Am. J. Phys. Anthropol.* **128**, 709-726 (2005).
- 467 17. Kaifu, Y., Aziz, F. & Baba, H. Hominin mandibular remains from Sangiran: 1952-1986
468 collection. *Am. J. Phys. Anthropol.* **128**, 497-519 (2005).
- 469 18. Schwartz, J.H. & Tattersall, I. Defining the genus *Homo*. *Science* **349**, 931-932 (2015).
- 470 19. Grimaud-Hervé, D. & Widianto, H. in *Origine des Peuplements et Chronologie des Cultures*
471 *Paléolithiques dans le Sud-Est Asiatique.* (eds Sémah, F., Falguères, C., Grimaud-Hervé, D. &
472 Sémah, A.M.) 331-358 (Artcom', Paris, 2001).
- 473 20. Begun, D.R. *A Companion to Paleoanthropology.* Wiley-Blackwell, Chichester (2013).
- 474 21. Fleagle, J.G., *Primate Adaptation and Evolution, 3rd Edition.* Elsevier, London (2013).
- 475 22. Teaford, M.F. & Ungar, P.S. in *Handbook of Palaeoanthropology, 2nd Edition* (eds Henke, W. &
476 Tattersall, I.) 1465-1494. (Springer, New York, 2015).
- 477 23. Kullmer, O., *et al.* Occlusal Fingerprint Analysis (OFA) - quantification of tooth wear pattern.
478 *Am. J. Phys. Anthropol.* **139**, 600-605 (2009).
- 479 24. Olejniczak, A.J., *et al.* Molar enamel thickness and dentine horn height in *Gigantopithecus*
480 *blacki*. *Am. J. Phys. Anthropol.* **135**, 85-91 (2008).
- 481 25. Fiorenza, L., Nguyen, N.H. & Benazzi, S. Stress distribution and molar macrowear in *Pongo*
482 *pygmaeus*: A new approach through Finite Element and Occlusal Fingerprint Analyses. *Hum.*

- 483 *Evol.* **30**, 215-226 (2015).
- 484 26. Zanolli, C. *et al.* The Early Pleistocene deciduous hominid molar FS-72 from the Sangiran
485 Dome of Java, Indonesia: A taxonomic reappraisal based on its comparative endostructural
486 characterization. *Am. J. Phys. Anthropol.* **157**, 666-674 (2015).
- 487 27. Smith, T.M. *et al.* Variation in enamel thickness within the genus *Homo*. *J. Hum. Evol.* **62**, 395-
488 411 (2012).
- 489 28. Kupczik, K., Olejniczak, A.J., Skinner, M.M & Hublin, J.J. Molar crown and root size
490 relationship in anthropoid primates. *Front. Oral Biol.* **13**, 16-22 (2009).
- 491 29. Skinner, M.M. *et al.* Dental trait expression at the enamel-dentine junction of lower molars in
492 extant and fossil hominoids. *J. Hum. Evol.* **54**, 173-186 (2008).
- 493 30. Schwartz, J. In *Homenaje al Dr. José Gibert Clois. Una vida dedicada a la ciencia y al*
494 *conocimiento de los primeros europeos* (ed Ribot, R.) 93-110 (Publicaciones Diputación de
495 Granada; Granada, 2016).
- 496 31. Simons, E. L. & Chopra, S. R. K. *Gigantopithecus* (Pongidae, Hominoidea) a new species
497 from North India. *Postilla* **138**, 1-18 (1969).
- 498 32. Wang, W. New discoveries of *Gigantopithecus blacki* teeth from Chuifeng Cave in the Buling
499 Basin, Guangxi, south China. *J. Hum. Evol.* **57**, 229-240 (2009).
- 500 33. Koufos, G.D. & de Bonis, L. New material of *Ouranopithecus macedoniensis* from late
501 Miocene of Macedonia (Greece) and study of its dental attrition. *Geobios* **39**, 223-243 (2006).
- 502 34. Xu, Q. & Lu, Q. *Lufengpithecus lufengensis – An Early Member of Hominidae*. Science Press,
503 Beijing (2007).
- 504 35. Smith, T.M., *et al.* Dental ontogeny in Pliocene and Early Pleistocene hominins. *PLoS One* **10**,
505 e0118118 doi:10.1371/journal.pone.0118118 (2015).
- 506 36. Smith, T.M. Dental development in living and fossil orangutans. *J. Hum. Evol.* **94**, 92-105
507 (2016).
- 508 37. Mahoney, P., Smith, T.M., Schwartz, G.T., Dean, M.C. & Kelley, J. Molar crown formation in
509 the Late Miocene Asian hominoids, *Sivapithecus parvada* and *Sivapithecus indicus*. *J. Hum.*
510 *Evol.* **53**, 61-68 (2007).
- 511 38. Schwartz, G.T., Liu, W. & Zheng, L. Preliminary investigation of dental microstructure in the
512 Yuanmou hominoid (*Lufengpithecus huidienensis*), Yunnan Province, China. *J. Hum. Evol.* **44**,
513 189-202 (2003).
- 514 39. Olejniczak, A.J., *et al.* Three-dimensional molar enamel distribution and thickness in
515 *Australopithecus* and *Paranthropus*. *Biol. Lett.* **4**, 406-410 (2008).
- 516 40. Noerwidi, S., Siswanto & Widiyanto, H. Giant primate of Java: A new *Gigantopithecus*
517 specimen from Samedo. *Berkala Arkeologi* **36**, 141-160 (2016).
- 518 41. Bettis III, E.A., *et al.* Way out of Africa: Early Pleistocene paleoenvironments inhabited by
519 *Homo erectus* in Sangiran, Java. *J. Hum. Evol.* **56**, 11-24 (2009).
- 520 42. Sémah, A.M., Sémah, F., Djubiantono, T. & Brasseur, B. Landscapes and hominids'
521 environments: Changes between the Lower and the early Middle Pleistocene in Java
522 (Indonesia). *Quat. Intl.* **223-224**, 451-454 (2010).
- 523 43. Janssen R., *et al.* Tooth enamel stable isotopes of Holocene and Pleistocene fossil fauna reveal
524 glacial and interglacial paleoenvironments of hominins in Indonesia. *Quat. Sci. Rev.* **144**, 145-
525 154 (2016).
- 526 44. Kelley, J. & Gao, F. Juvenile hominoid cranium from the late Miocene of southern China and
527 hominoid diversity in Asia. *Proc. Natl. Acad. Sci. USA.* **109**, 6882–6885 (2012).
- 528 45. Ji, X-P., *et al.* Juvenile hominoid cranium from the terminal Miocene of Yunnan, China. *Chin.*
529 *Sci. Bull.* **58**, 3771-3779 (2013).
- 530 46. Nater, A. *et al.* Morphometric, behavioral, and genomic evidence for a new orangutan species.
531 *Curr. Biol.* **27**, 1-12 (2017).
- 532 47. Kardjilov, N., *et al.* New features in cold neutron radiography and tomography. Part II: applied
533 energy-selective neutron radiography and tomography. *Nucl. Instr. Meth. Phys. Res. A* **501**,
534 536-546 (2003).

- 535 48. Tremsin, A.S., *et al.* High resolution neutron imaging capabilities at BOA beamline at Paul
536 Scherrer Institut. *Nucl. Instr. Meth. Phys. Res. A* **784**, 486-493 (2015).
- 537 49. Winkler, B. Applications of neutron radiography and neutron tomography. *Rev. Min. Geochem.*
538 **63**, 459-471 (2006).
- 539 50. Schwarz, D., Vontobel, P., Lehmann, E.H., Meyer, C.A. & Bongartz, G. Neutron tomography of
540 internal structures of vertebrate remains: a comparison with X-ray computed tomography.
541 *Palaeontol. Electronica* **8** http://palaeo-electronica.org/2005_2/neutron/issue2_05.htm (2005).
- 542 51. Sutton, M.D. Tomographic techniques for the study of exceptionally preserved fossils. *Proc. R.*
543 *Soc. B* **275**, 1587-1593 (2008).
- 544 52. Spoor, C.F., Zonneveld, F.W. & Macho, G.A. Linear measurements of cortical bone and dental
545 enamel by computed tomography: applications and problems. *Am. J. Phys. Anthropol.* **91**, 469-
546 484 (1993).
- 547 53. Fajardo, R.J., Ryan, T.M. & Kappelman, J. Assessing the accuracy of high-resolution X-ray
548 computed tomography of primate trabecular bone by comparisons with histological sections.
549 *Am. J. Phys. Anthropol.* **118**, 1-10 (2002).
- 550 54. Coleman, M.N. & Colbert, M.W. CT thresholding protocols for taking measurements on three-
551 dimensional models. *Am. J. Phys. Anthropol.* **133**, 723-725 (2007).
- 552 55. Beaudet, A., *et al.* Neutron microtomography-based virtual extraction and analysis of a
553 cercopithecoid partial cranium (STS 1039) embedded in a breccia fragment from Sterkfontein
554 Member 4 (South Africa). *Am. J. Phys. Anthropol.* **159**, 737-745 (2016).
- 555 56. Zanolli, C., *et al.* Exploring hominin and non-hominin primate dental fossil remains with
556 neutron microtomography. *Physics Procedia* **88**, 109-115 (2017).
- 557 57. Mills, J.R.E. Ideal dental occlusion in the primates. *Dental Practitioner* **6**, 47-63 (1955).
- 558 58. Hiiemae, K.M. & Kay, R.F. in *Craniofacial Biology of Primates, 4th International Congress of*
559 *Primates, Vol. 3* (eds Montagna, W. & Zingesser, M.R.), 28-64 (Karger, Beaverton, 1973)
- 560 59. Kay, R.F. & Hiiemae, K.M. Jaw movement and tooth use in recent and fossil primates. *Am. J.*
561 *Phys. Anthropol.* **40**, 227-256 (1974).
- 562 60. Maier, W. & Schneck, G. Konstruktionsmorphologische Untersuchungen am Gebiß der
563 hominoiden Primaten. *Zeitschrift für Morphologie und Anthropologie* **72**, 127-169 (1981).
- 564 61. Ulhaas, L., Kullmer, O. & Schrenk, F. In: *Dental Perspectives on Human Evolution: State of*
565 *the Art Research in Dental Paleoanthropology* (eds Bailey, S.E. & Hublin, J.J.) 369-390.
566 (Springer, Dordrecht, 2007).
- 567 62. Kullmer, O., Schulz, D. & Benazzi, S. An experimental approach to evaluate the
568 correspondence between wear facet position and occlusal movements. *Anat. Rec.* **295**, 846-852
569 (2012).
- 570 63. von Koenigswald, W., Anders, U., Engels, S., Schultz, J.A. & Kullmer, O. Jaw movement in
571 fossil mammals: analysis, description and visualization. *Paläontologische Zeitschrift* **87**, 141-
572 159 (2013).
- 573 64. Fiorenza, L., *et al.* Molar macrowear reveals Neanderthal ecogeographic dietary variation.
574 *PLoS One* **6**, e14769 <http://dx.doi.org/10.1371/journal.pone.0014769> (2011).
- 575 65. Janis, C.M. in *Evolutionary Paleobiology of Behavior and Coevolution* (ed Boucot, A.J.) 241-
576 259 (Elsevier Science, Amsterdam, 1990).
- 577 66. Hamilton, N. ggtern: An extension to 'ggplot2', for the creation of ternary diagrams. R package
578 version 2.2.2. <https://CRAN.R-project.org/package=ggtern> (2017).
- 579 67. R Development Core Team. *R: A language and environment for statistical computing.*
580 <http://www.R-project.org>. (2017).
- 581 68. Hervé, M. RVAideMemoire: Diverse Basic Statistical and Graphical Functions. R package
582 version 0.9-66. <https://CRAN.R-project.org/package=RVAideMemoire> (2017).
- 583 69. Olejniczak, A.J. *et al.* Dental tissue proportions and enamel thickness in Neandertal and
584 modern human molars. *J. Hum. Evol.* **55**, 12-23 (2008).
- 585 70. Kupczik, K., & Dean, M.C. Comparative observations on the tooth root morphology of
586 *Gigantopithecus blacki*. *J. Hum. Evol.* **54**, 196-204 (2008).

- 587 71. Maureille, B., Rougier, H., Houët, F. & Vandermeersch, B. Les dents inférieures du
588 néandertalien Regourdou 1 (site de Regourdou, commune de Montignac, Dordogne): analyses
589 métriques et comparatives. *Paleo* 13, 183-200 (2001).
- 590 72. Scolan, H., Santos, F., Tillier, A.M., Maureille, B. & Quintard, A. Des nouveaux vestiges
591 néanderthaliens à Las Pélénos (Monsempron-Libos, Lot-et-Garonne, France). *Bull. Mém. Soc.*
592 *Anthropol. Paris* 24, 69-95 (2012).
- 593 73. Macchiarelli, R., Bondioli, L. & Mazurier, A. in: *Technique and Application in Dental*
594 *Anthropology* (eds Irish, J.D. & Nelson, G.C.) 426-448 (Cambridge University Press,
595 Cambridge, 2008).
- 596 74. Macchiarelli, R., Bayle, P., Bondioli, L., Mazurier, A. & Zanolli, C. in *Anthropological*
597 *Perspectives on Tooth Morphology. Genetics, Evolution, Variation* (eds Scott, G.R., Irish, J.D.)
598 250-277 (Cambridge University Press, Cambridge, 2013).
- 599 75. Bayle, P., *et al.* In: *Pleistocene Databases. Acquisition, Storing, Sharing* (eds Macchiarelli, R.
600 & Weniger, G.C.) 29-46 (Wissenschaftliche Schriften des Neanderthal Museums 4, Mettmann,
601 2011).
- 602 76. Zanolli, C., Bayle, P. & Macchiarelli, R. Tissue proportions and enamel thickness distribution
603 in the early Middle Pleistocene human deciduous molars from Tighenif (Ternifine), Algeria.
604 *C.R. Palevol* 9, 341-348 (2010).
- 605 77. Zanolli, C. Molar crown inner structural organization in Javanese *Homo erectus*. *Am. J. Phys.*
606 *Anthropol.* 156, 148-157 (2015).
- 607 78. Mitteroecker, P. & Bookstein, F.L. Linear discrimination, ordination, and the visualization of
608 selection gradients in modern morphometrics. *Evol. Biol.* 38, 100-114 (2011).
- 609 79. Dray, S. & Dufour, A.B. The ade4 package: implementing the duality diagram for ecologists. *J.*
610 *Stat. Softw.* 22, 1-20 (2007).
- 611 80. Bookstein, F.L. *Morphometric Tools for Landmark Data: Geometry and Biology* (Cambridge
612 University Press, Cambridge, 1991).
- 613 81. Gokcen, I. & Peng, J. Comparing Linear Discriminant Analysis and Support Vector Machines.
614 In: *Advances in Information Systems: Second International Conference, ADVIS 2002* (eds
615 Yakhno, T.) 104-113 (Springer-Verlag, Berlin, 2002).
- 616

617 **Acknowledgements**

618 We thank the Pusat Penelitian Arkeologi of Jakarta and the Balai Pelestarian Situs Manusia Purba
619 of Sangiran, Java, and the French MNHN. We thank the many curators and colleagues who granted
620 access to fossil and recent hominid materials for scanning. We are grateful to D. Grimaud-Hervé, C.
621 Hertler, F. Sémah and H. Widiyanto for support. We thank J. Braga for sharing the
622 microtomographic scans of South African fossil specimens. For scientific discussion, we thank P.
623 Bayle, S. Benazzi, L. Bondioli, J. Braga, M.C. Dean, F. Détroit, Y. Hou, L. Mancini, B. Maureille,
624 A. Mazurier, L. Puymeraul, L. Rook, C. Tuniz, B. Wood. We would like to express our gratitude to
625 C. Hemm, L. Hauser, M. Janocha, L. Strzelczyk for their help with the surface scanning and OFA
626 analysis. Scanning of the Vietnamese specimens was funded by the PICS-CNRS to AMB. Research
627 supported by the French CNRS.

628

629 **Author Contributions**

630 The study was initiated by C.Z. during his PhD research project under the supervision of R.M.
631 Microtomographic-based data were collected and elaborated by C.Z., A.M.B., F.D., J.K., O.K.,
632 A.T.N., K.T.N., B.S., J.-J.H., M.M.S., J.X. and R.M. Quantitative data were compiled and analysed
633 by C.Z., J.D., O.K., L.P., M.M.S and R.M. C.Z, R.M, O.K. and J.K. wrote the manuscript with
634 contributions from all other authors.

635

636 **Competing interests**

637 The authors declare no competing interests.

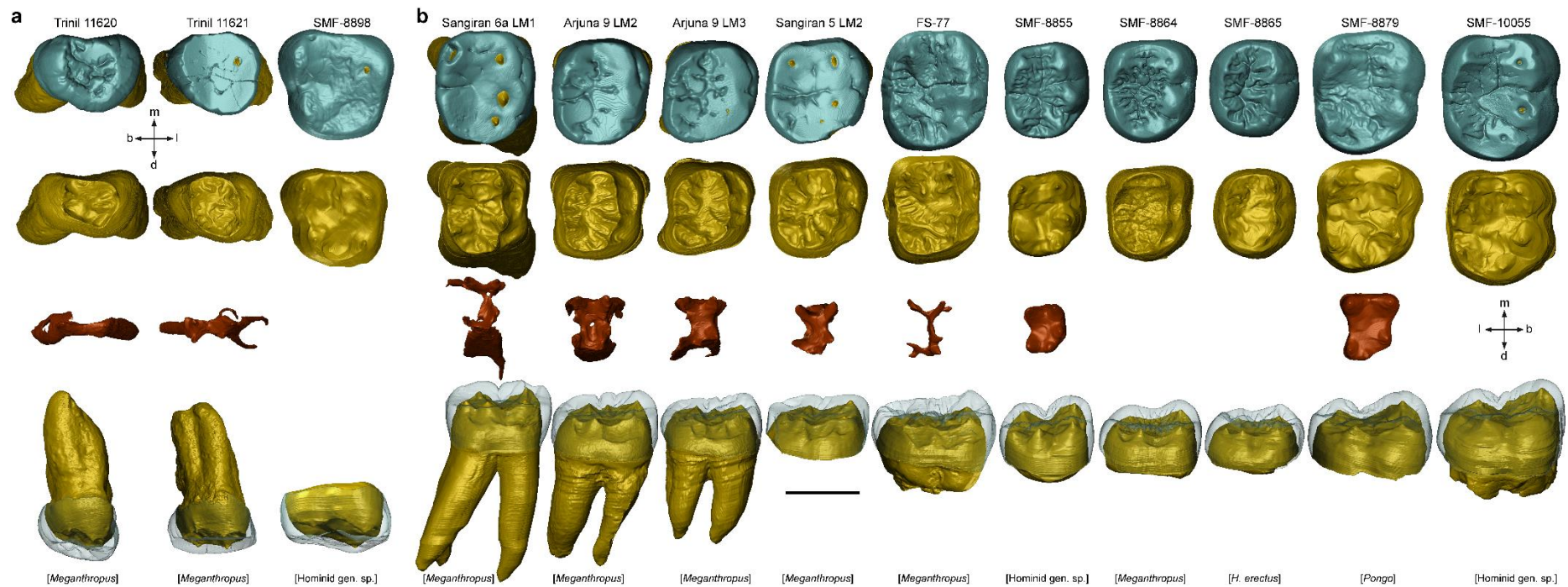
638

639 **Additional Information**

640 **Correspondence and requests for materials** should be addressed to C.Z.

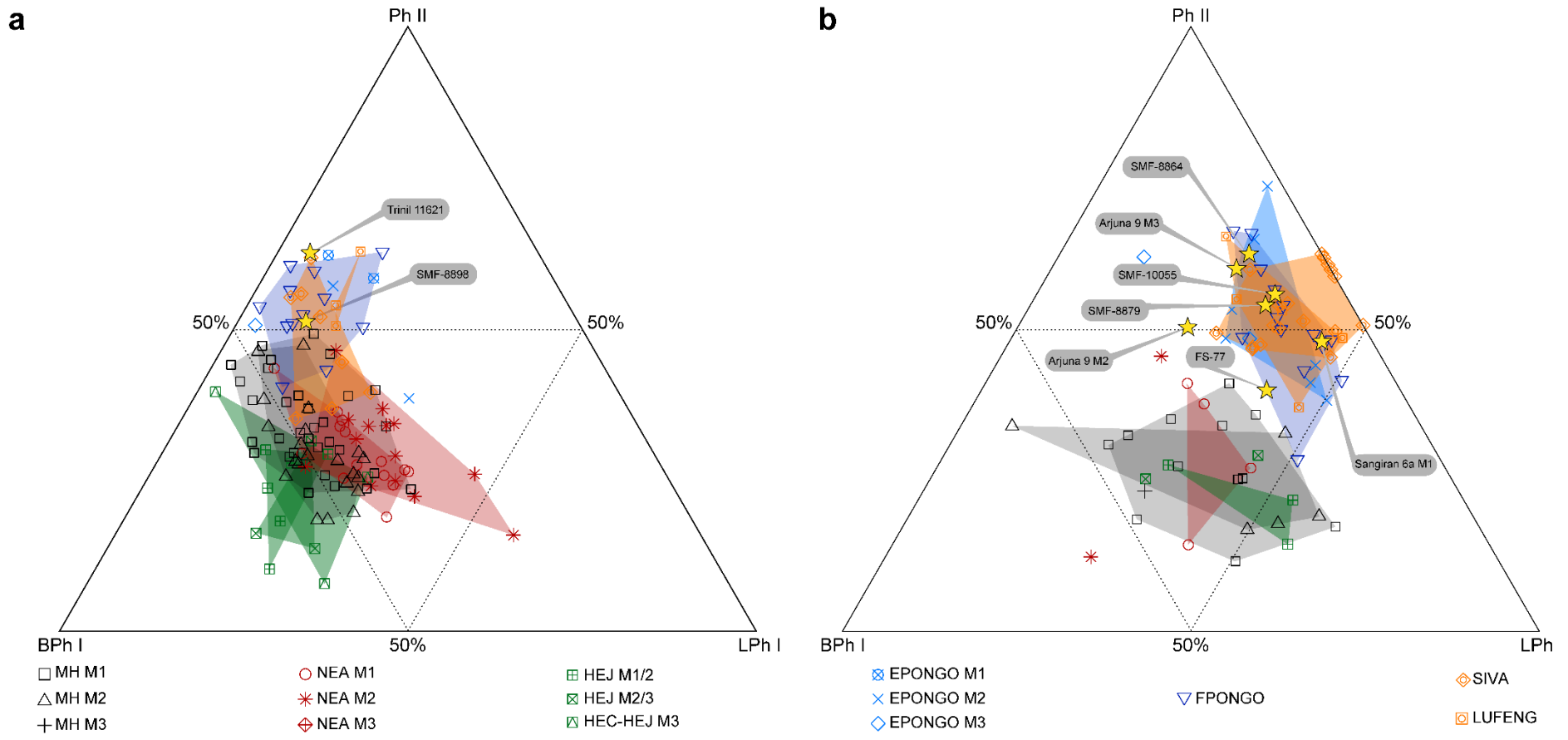
641 (clement.zanolli@gmail.com).

642



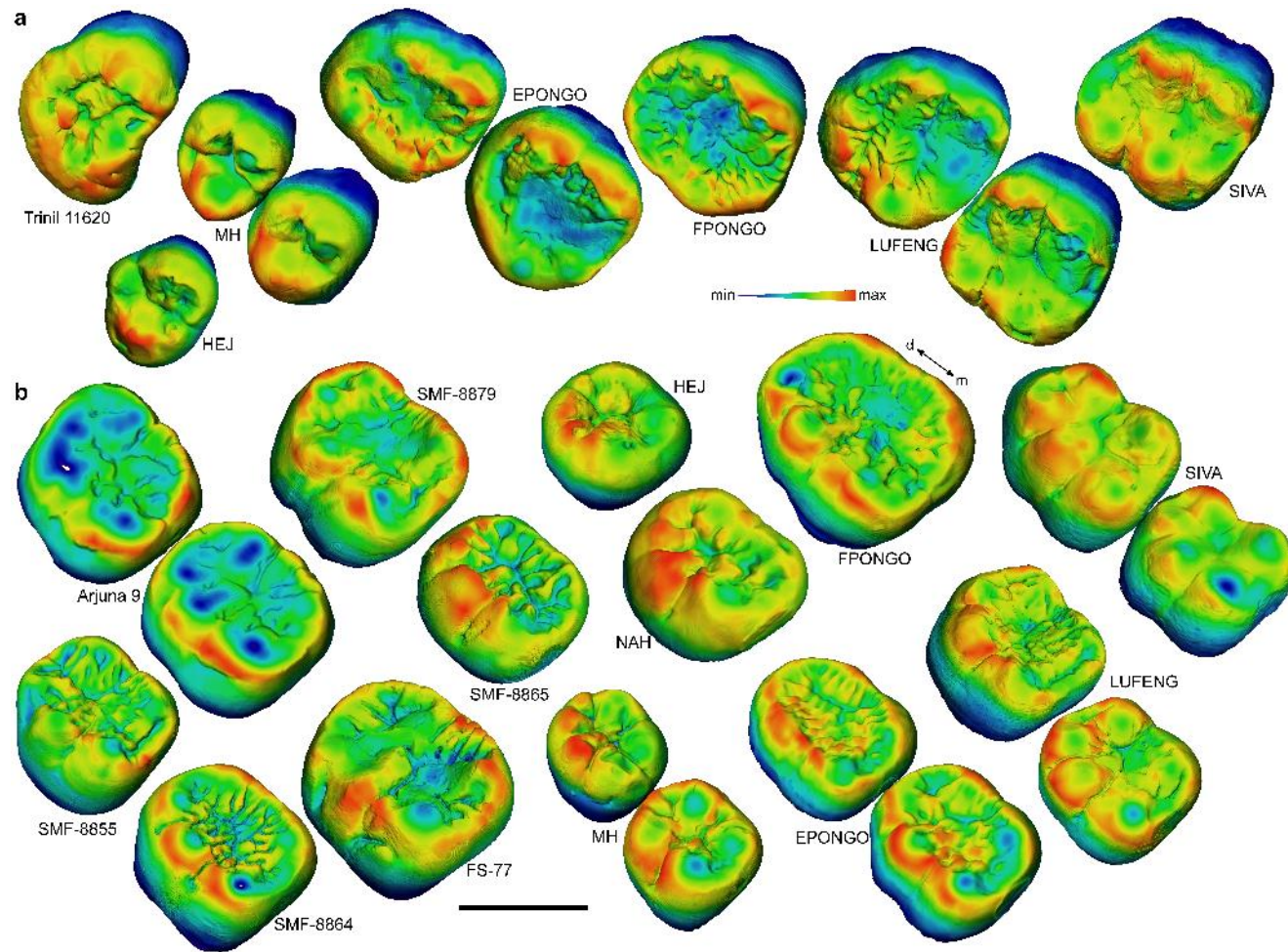
644
 645
 646
 647
 648
 649
 650
 651

Figure 1 | Virtual rendering of the Indonesian hominid teeth examined for taxonomic reassessment. **a**, Maxillary molars. **b**, Mandibular molars (Supplementary Table 1). From the top, the rows show: the external occlusal morphology, the occlusal dentine, the occlusal pulp cavity and the EDJ with the overlain semi-transparent enamel cap in buccal view. For SMF-8879, only the crown is imaged. For Trinil 11621, Sangiran 5 and 6a, the worn dentine horn apices were reconstructed following the morphology of the other well-preserved cusps (see Methods). **b**, buccal; **d**, distal; **l**, lingual; **m**, mesial. Scale bar, 10 mm.



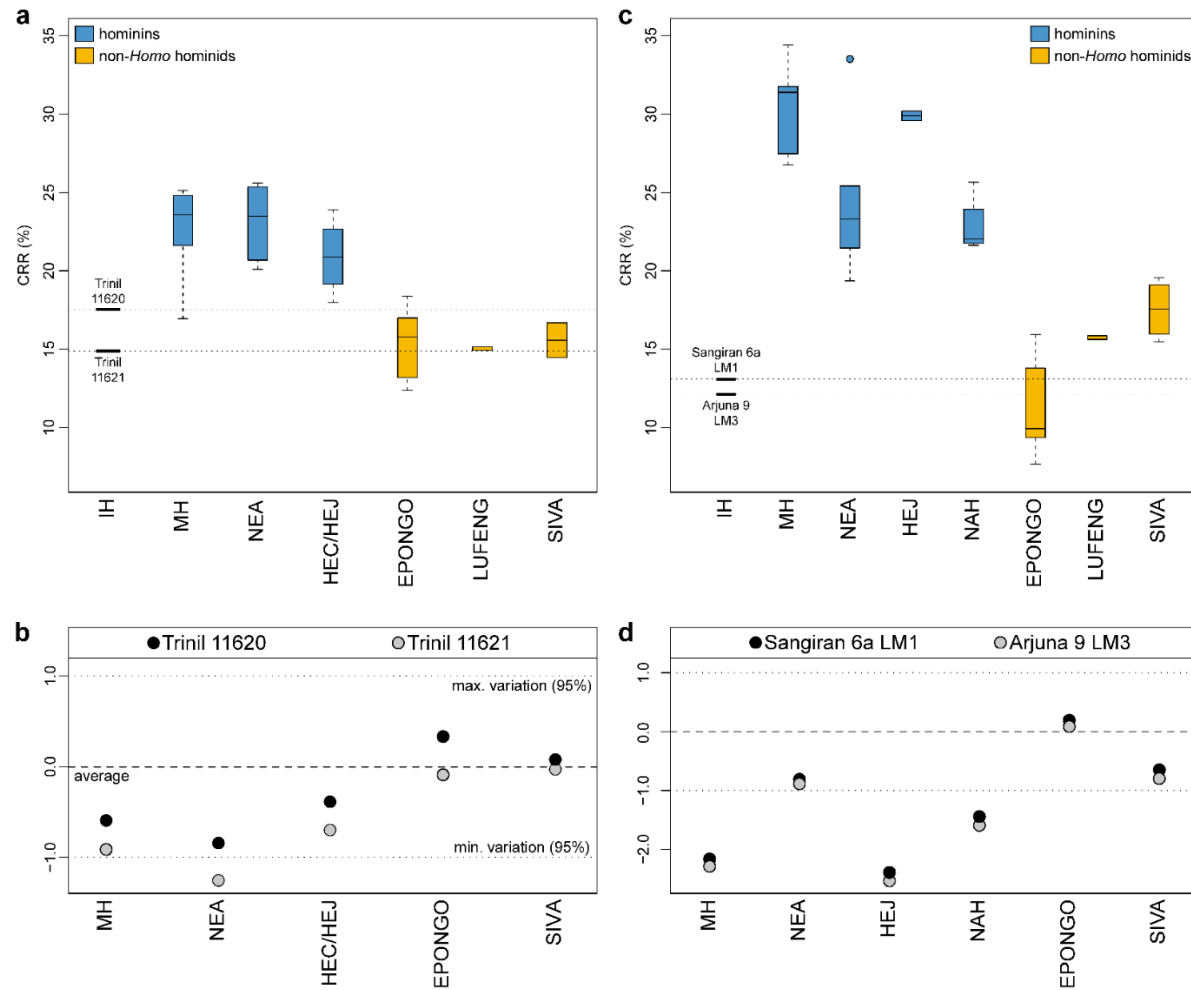
652
653
654
655
656
657
658
659

Figure 2 | Occlusal Fingerprint Analyses. **a, b**, Ternary diagram showing the proportions (in %) of relative wear areas of buccal phase I (BPh I), lingual phase I (LPh I), and phase II (Ph II) facets for the Indonesian fossil hominid maxillary (**a**) and mandibular (**b**) molars (Supplementary Table 1) compared with fossil and extant hominid specimens/samples. Each base of the triangle represents a ratio of 0% while the vertices correspond to a percentage of 100%. EPONGO, extant *Pongo*; FPONGO, fossil *Pongo*; HEC, *H. erectus* from China; HEJ, *H. erectus* from Java; LUFENG, *Lufengpithecus*; MH, modern humans; NEA, Neanderthals; SIVA, *Sivapithecus* (Supplementary Table 2).



660
661

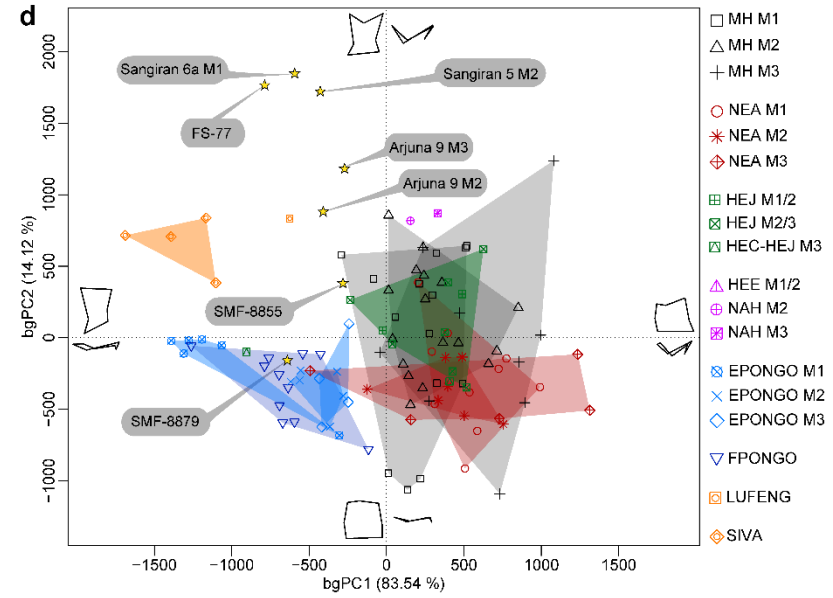
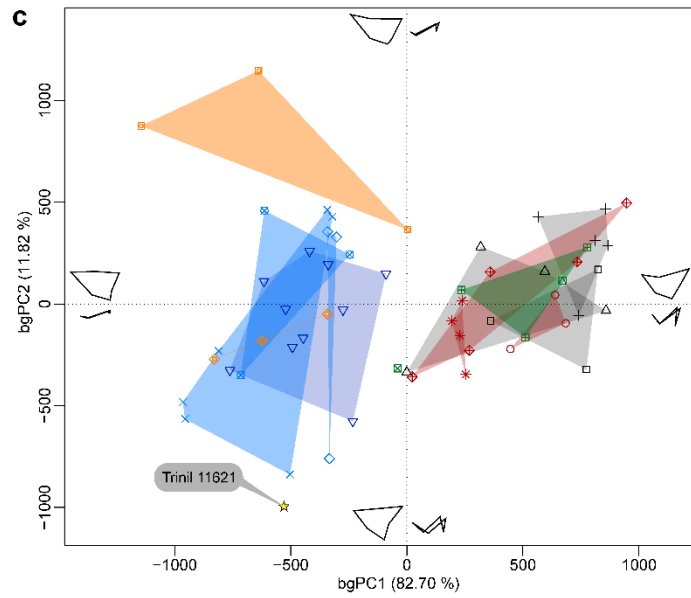
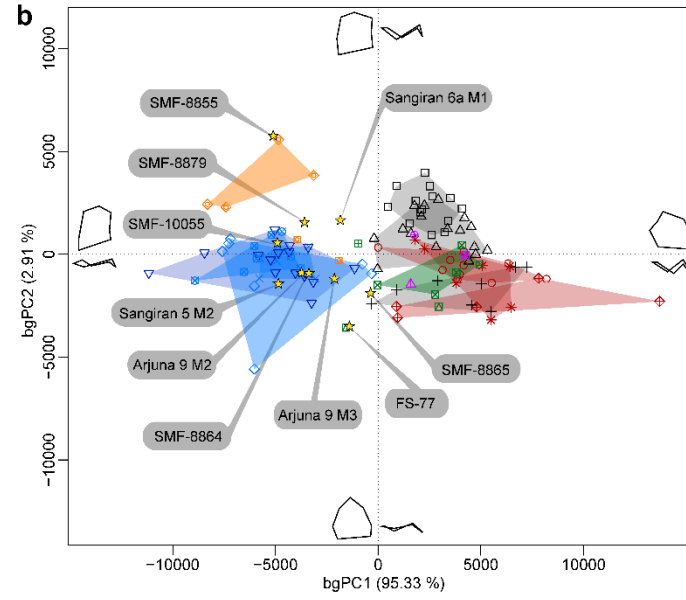
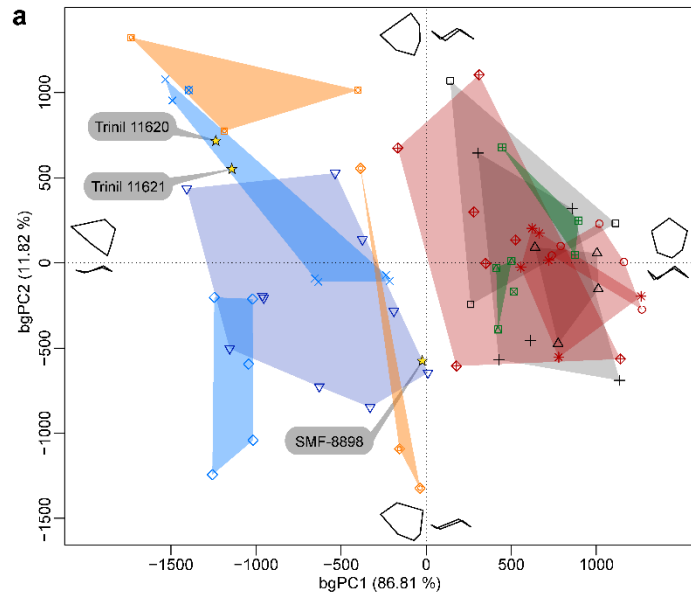
662 **Figure 3 | Enamel thickness cartographies.** **a**, Maxillary molars, **b**, Mandibular molars. The Indonesian hominid teeth (Supplementary Table 1)
663 are compared with fossil and extant hominid specimens. EPONGO, extant *Pongo*; FPONGO, fossil *Pongo*; HEJ, *H. erectus* from Java;
664 LUFENG, *Lufengpithecus*; MH, modern humans; NAH, North African late Early Pleistocene *Homo*; SIVA, *Sivapithecus* (Supplementary Table
665 2). Irrespective of their original side, all specimens are displayed as right anteriors in a slightly oblique occlusal perspective. Scale bar, 10 mm.



666
667

668 **Figure 4 | Molar crown-root proportions.** **a, b**, The crown-root ratio (CRR, in %) and its adjusted Z-score statistics for the Indonesian hominid
669 (IH) maxillary molars from Trinil compared with fossil and extant hominid specimens/samples. **c, d**, Similar comparative analyses for the
670 mandibular molars of Sangiran 6a and Arjuna 9 (Supplementary Table 1). The boxplots show the median, the 25th and 75th percentiles (upper and
671 lower hinges), and the range (lower and upper whiskers). EPONGO, extant *Pongo*; HEC, *H. erectus* from China; HEJ, *H. erectus* from Java;
672 LUFENG, *Lufengpithecus*; MH, modern humans; NAH; North African late Early *Homo*; NEA, Neanderthals; SIVA, *Sivapithecus*

673 (Supplementary Table 2).



675

676

677

678

679

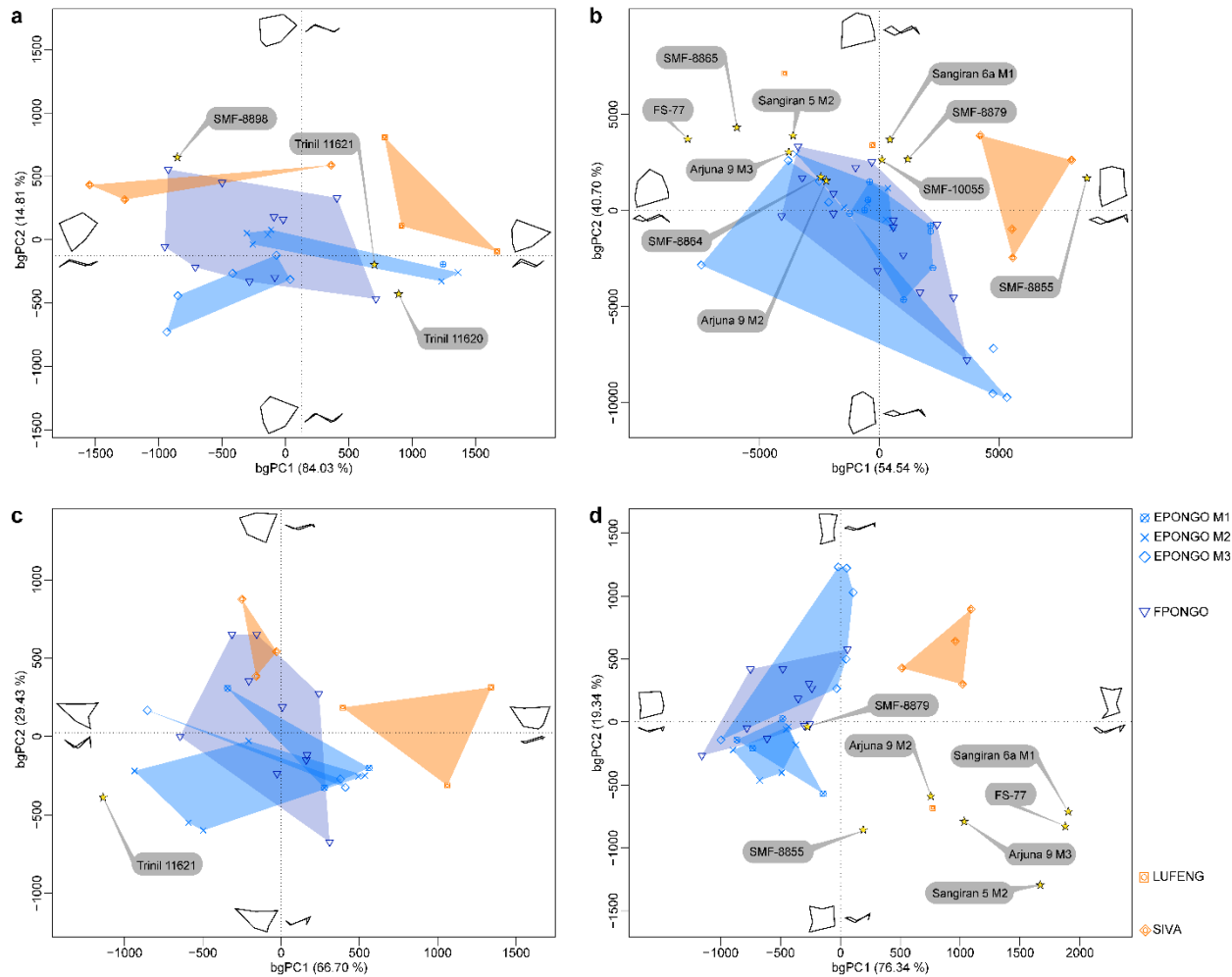
680

681

682

683

Figure 5 | Geometric morphometric analyses of the EDJ and pulp chamber. a, b, Between-group principal component analyses (bgPCA) of the 3D landmarks Procrustes-registered shape coordinates of the Indonesian hominid maxillary (**a**) and mandibular (**b**) molar EDJs (Supplementary Table 1) compared with fossil and extant hominid specimens/samples. **c, d,** bgPCA of the underlying maxillary (**c**) and mandibular (**d**) pulp cavity. The wireframes at the end of the axes illustrate the extreme morphological variation trends along each bgPC in occlusal (mesial aspect upward) and buccal views (mesial aspect rightward). EPONGO, extant *Pongo*; FPONGO, fossil *Pongo*; HEC, *H. erectus* from China; HEE, *H. erectus/ergaster* from Eritrea; HEJ, *H. erectus* from Java; LUFENG, *Lufengpithecus*; MH, modern humans; NAH, North African late Early Pleistocene *Homo*; NEA, Neanderthals; SIVA, *Sivapithecus* (Supplementary Table 2).



684
685
686
687
688
689
690

Figure 6 | Geometric morphometric analyses of the EDJ and pulp chamber in non-*Homo* hominids. **a, b,** Between-group principal component analyses (bgPCA) of the 3D landmarks Procrustes-registered shape coordinates of the Indonesian hominid maxillary (**a**) and mandibular (**b**) molar EDJs (Supplementary Table 1) compared with fossil and extant non-*Homo* hominid samples. **c, d,** bgPCA of the underlying maxillary (**c**) and mandibular (**d**) pulp cavity. The wireframes at the end of the axes illustrate the extreme morphological variation trends along each bgPC in occlusal (mesial aspect upward) and buccal views (mesial aspect rightward). EPONGO, extant *Pongo*; FPONGO, fossil *Pongo*;

691 LUFENG, *Lufengpithecus*; SIVA, *Sivapithecus* (Supplementary Table 2).
692